Evidence for elevation-dependent warming from the Chinese Tianshan Mountains

Lu Gao[1,2,3,4], Haijun Deng[1,2,3,4], Xiangyong Lei[3], Jianhui Wei[5], Yaning Chen[6], Zhongqin Li[7], Miaomiao Ma[8], Xingwei Chen[1,2,3,4], Ying Chen[1,2,3,4], Meibing Liu[1,2,3,4], Jianyun Gao[9]

[1]Institute of Geography, Fujian Normal University, Fuzhou 350007, China
[2]Fujian Provincial Engineering Research Center for Monitoring and Assessing Terrestrial Disasters, Fujian Normal University, Fuzhou 350007, China
[3]College of Geographical Sciences, Fujian Normal University, Fuzhou 350007, China
[4]State Key Laboratory of Subtropical Mountain Ecology (Funded by the Ministry of Science and Technology and the Fujian province), Fujian Normal University, Fuzhou 350007, China
[5]Institute of Meteorology and Climate Research (IMK-IFU), Karlsruhe Institute of Technology, Campus Alpine, Garmisch-Partenkirchen 82467, Germany
[6]State Key Laboratory of Desert and Oasis Ecology, Xinjiang Institute of Ecology and Geography, Chinese Academy of Sciences, Urumqi 830011, China
[7]State Key Laboratory of Cryospheric Sciences/Tianshan Glaciological Station, Northwest Institute of Eco-Environment and Resources, Chinese Academy of Sciences, Lanzhou 730000, China
[8]China Institute of Water Resources and Hydropower Research, Beijing 100038, China
[9]Fujian Key Laboratory of Severe Weather, Fuzhou 350001, China

Correspondence to: Lu Gao (l.gao@foxmail.com)

Abstract. The phenomenon that the warming rate of air temperature is amplified with elevation is termed elevation-dependent warming (EDW). It has been clarified that EDW can accelerate the retreat of glaciers and the melting of snow, which would have significant impacts on regional ecological environment. Owing to the lack of high-density ground observations in the high mountains, there is a widespread controversy on the existence of the EDW. Current evidences are mainly derived from some typical high mountains such as the Swiss Alps, the Colorado Rocky Mountains, the Tropical Andes and the Tibetan Plateau/Himalayas. Rare evidences in other mountains have been reported, especially in arid regions. In this study, EDW features (regional warming amplification and altitude warming amplification) in the Chinese Tianshan Mountains (CTM) are detected using a unique high-resolution (1 km, 6-hourly) air temperature data set (CTMD) from 1979-2016. The results showed that there are significant EDW signals at different altitudes on different time scales. The CTM show significant regional warming amplification in spring, especially in March, which has greater warming trends than continental China with respect to three temperatures (minimum temperature, mean temperature and maximum temperature). The warming rate of the minimum temperature in winter shows significant elevation dependence ($p<0.01$), especially above 4000 m. The greatest altitudinal gradient in the warming rate of maximum temperature is found above 2500 m in April. For the mean temperature, the warming rates in January, February and March show prominent altitude warming amplification but with different significances. Within the CTM, the Tolm Mountains, the eastern part of the Borokoonu Mountains, the Bogda Mountains and the Balikun Mountains are the representative regions that show significant altitude warming

amplification on different time scales. This new evidence could partly explain the accelerated melting of snow in the CTM, though the mechanisms remain to be explored.

1 Introduction

The elevation-dependent warming (EDW) indicates that the warming rate of air temperature is amplified with elevation,
40 especially in the high mountain regions. Two basic characteristics, regional warming amplification and altitude warming amplification are judged as the "fundamental questions" of the EDW by Rangwala and Miller (2012). The regional warming amplification means the warming rate of air temperature in a certain mountain is greater compared to other regions outside this mountain. The altitude warming amplification means the warming rate is greater in the high-altitude areas than the low-altitude areas within the same mountain. However, owing to the high sensitivity of glaciers and snow to climate change,
45 mountains are regarded as the outposts of global climate change (Sorg et al., 2012). Previous studies have reported the potential widespread existence of the elevation-dependent warming (EDW) phenomenon, which is an ideal early indicator of climate warming in mountain systems under global climate change (Dong et al., 2015). EDW could accelerate the changes in the mountain ecosystems, cryosphere systems, water cycles and biodiversity, leading to irreversible and profound impacts on the regional ecological environment and socioeconomic development (Mountain Research Initiative EDW Working Group,
50 2015; Rangwala and Miller, 2012). Therefore, the detection and exploration of the spatial and temporal differentiation characteristics of EDW not only plays an inestimable and important role in the in-depth understanding of regional climate change and in improving the predictive ability of mountain climate, but also in maintaining the relative stability and ecological balance of these natural mountain ecosystems.

Current evidence for the EDW phenomenon mainly stem from multi-source data detections and regional climate models.
55 The main data resources include ground meteorological stations, radiosonde, reanalysis, and remote sensing data. For example, the warming rate has been found to be more intense in the high-altitude regions of Western Europe and Asia based on a global high-altitude observation data set (Diaz and Bradley, 1997). The significant EDW phenomenon of the annual maximum and minimum temperatures in the Alps has been detected based on ground observation sites (Beniston and Rebetez, 1996). The temperatures in the Alps at different altitudes show distinctly different seasonal trends. The minimum
60 temperature rises faster at high altitudes than at low altitudes (Jungo and Beniston, 2001). A significant EDW phenomenon for the annual mean temperature in tropical alpine areas has been detected based on global radiosonde data (Seidel and Free, 2003). The warming trends for the maximum and minimum temperatures show significant elevation dependence in the 2000–4000 m altitude range of the Rocky Mountains (Diaz and Eischeid, 2007; Mcguire et al., 2012). The climate warming trend for the Qinghai-Tibet Plateau from 1961 to 1990 was proportional to the altitude, especially in winter (Liu and Hou,
65 1998). In the high-altitude areas (above 4000 m) of the Qinghai-Tibet Plateau, the increment in the mean temperature over four seasons and on the annual scale is greater than that in the low-altitude areas (Du, 2001); the temperature warming rate

increases by 0.16 ℃ 10a^{-1} for every 1 km increment in altitude (Wang et al., 2012). An observation data set contains 139 weather stations showed warmer trends at 4000 m (0.5 ℃ 10a^{-1}) and 3000 m (0.357 ℃ 10a^{-1}) than that at 2000 m (0.316 ℃ 10a^{-1}) with respect to annual mean temperature in the Tibetan Plateau from 1961-2012 (Yan and Liu, 2014). In general, from

70 a regional perspective, the European Alps, Himalayas-Tibetan Plateau, South American Andes, and North American Rocky Mountains are hotspots for the EDW studies (Wang et al., 2014; Thakuri et al., 2019; Guo et al., 2019; Pepin et al., 2019). From the perspective of significance of the EDW, the seasonal scale is more significant than the annual scale because of the significant changes in climate drivers such as snow/ice cover, clouds and others at different elevations (Mountain Research Initiative EDW Working Group, 2015; Rangwala and Miller, 2012). Furthermore, the warming rate of minimum temperature

75 is greater than that for maximum and mean temperatures (Rangwala and Miller, 2012; Mountain Research Initiative EDW Working Group, 2015).

Although many studies have detected EDW phenomena in different mountains globally, there is still widespread controversy and no consensus has been reached on the existence of EDW. The main reason behind this is the scarcity of ground observation data, especially in mountains above 3000 m (Rangwala and Miller, 2012; Mountain Research Initiative EDW

80 Working Group, 2015). Even the detection of EDW is different within the same mountain that uses different observations (i.e. different number of sites or different site locations). For example, some studies have shown a significant prevalence of EDW since the second half of the 20th century over the Tibetan Plateau (Liu et al., 2009; Rangwala et al., 2009). However, an analysis claimed that the EDW over the Qinghai-Tibet Plateau is not significant based on the observations from 71 ground stations and 56 reanalysis grids (NCEP and ERA-40 grid with a spatial resolution of 2.5 °×2.5 °) data (You et al.,

85 2010). Similarly, EDW has been found to be not significant at altitudes above 5000 m based on the observations from 25 ground stations and 0.5 ° grid data combined with WRF model simulations (Gao et al., 2018b). Although satellite data compensates for the deficiencies of ground observation stations to a large extent, the associated relative short time series, long revisiting cycle, and image interpretation and inversion errors limit the reliability of EDW signal detection. It can be concluded that a uniform high-resolution air temperature dataset is the basic premise for accurate EDW detection.

90 As the farthest mountain system from the ocean, and the largest mountain system in the arid regions of the world, the Tianshan Mountain system is extremely important for assessing the climate change and ecological environment in north-western China and the entire nation because of its special geographical location and complex terrain (Chen et al., 2016). As the "water tower" of Central Asia, the Tianshan Mountain system not only breeds many rivers, but also produces a unique desert oasis ecosystem (Sorg et al., 2012; Chen et al., 2016). There are approximately 9035 glaciers with an area of ~9225

95 km^2 and water resources of 1011 km^3 in the Chinese Tianshan Mountains (CTM, Fig. 1) (Shi et al., 2009). However, in recent years, most glaciers in the CTM are in a state of accelerated degradation due to climate warming (Ding et al., 2006; Chen et al., 2016; Sorg et al., 2012). The warming rate in the CTM has reached 0.32–0.42 ℃10a^{-1} in the past 50 years, which is much higher than the national average (Gao et al., 2018a; Xu et al., 2018). However, EDW in the CTM still lacks

systematic detection. Current research on climate warming in the CTM does not provide sufficient solid evidence for the
100   EDW phenomenon. Therefore, in this study, EDW features in the CTM are comprehensively and systematically detected
based on a unique high-resolution (1 km, 6-hourly) air temperature dataset (hereafter referred to as CTMD) (Gao et al.,
2018a). The present study reveals the EDW characteristics for different temperature indicators on different time scales.

2 Data and Methods

2.1 CTMD

105   Lack of sufficient ground observations is the biggest obstacle to accurate detection of the EDW phenomenon. This is exactly
one of the original intentions of the CTMD development. Previous studies have shown that the ECMWF's third generation
reanalysis product, ERA-Interim has a relative small large-scale error (±2.5 K) and it could capture the annual and seasonal
climatologies very well (Gao et al., 2012, 2014, 2017; Simmons et al., 2010). The system bias of ERA-Interim is mainly
from the height discrepancy between ERA-Interim model height and observations (Gao et al., 2012, 2014, 2017). Thus, the
110   bias could be significant reduced for local climate trend investigation via an appropriate elevation correction procedure. A
robust approach based on internal vertical lapse rates derived from different ERA-Interim pressure levels was developed for
downscaling 0.25 ° grid ERA-Interim temperature to 1 km grid derived from SRTM (Gao et al., 2018a). This scheme is fully
independent of meteorological stations via Equation (1).

$$T_{1km} = T_{ERA\_025} + \Gamma \times \Delta h \tag{1}$$

115   T_{ERA_025} is the original 6-hourly ERA-Interim 2-m temperature at 0.25 ° grid. Γ describes the ERA-Interim internal lapse rates
derived from the temperatures and geopotential heights at different pressure levels. For example, Γ_{500_700} indicates the lapse
rate between 500 hPa and 700 hPa pressure level, which is calculated by the temperature differences divided by geopotential
height differences between these two pressure levels. Δh is the height difference between ERA-Interim model height and 1
km grid. Different Γ were used according to the altitude of 1 km grid. In other words, if the 1 km grid is lower than 1500 m
120   in altitude, Γ_{850_925} is applied because the geopotential height between 850 and 925 hPa pressure level ranges from 150 m to
1500 m. If a grid altitude is higher than 4000 m, Γ_{500_600} is applied for the downscaling model. The geopotential height at 850
and 700 hPa pressure levels is the demarcation for the altitude of 1500 m and 3000 m, respectively. In total, four lapse rates
(Γ_{500_600}, Γ_{600_700}, Γ_{700_850} and Γ_{850_925}) were used for different altitude ranges according to the 1 km grids (Gao et al., 2018a).
Therefore, the unique high-resolution (1 km, 6-hourly) air temperature dataset (CTMD) for the Chinese Tianshan Mountains
125   from 1979 to 2016 is at 1 km spatial resolution (total 356133 grids) with six-hourly time step at 00, 06, 12, and 18 UTC.
More information on the downscaling scheme and the CTMD could be found at Gao et al (2012, 2017, 2018a).

Although, the CTMD was validated by 24 meteorological stations on a daily scale, indicating a high reliability for the climatology trend investigations, the limitations should be fully demonstrated. Whether the lapse rate can accurately reflect the temperature changes at all altitudes is worth discussing. For example, the lapse rates of ERA-Interim are greater than observations from September to December, while lapse rate in the free atmosphere is steeper than that near surface because of the different radiation mechanism (Gao et al., 2018a). The lapse rate may be positive rather than negative since the "Cold Lake" effect in winter such as in the Turfan Basin, which may have a temperature inversion layer at night. Under this situation, the downscaling model may be disabled for winter. Therefore, an opposite trend for minimum temperature during winter is captured by the CTMD compared to the slight positive warming trend from 24 observation sites. Meanwhile, the trend of diurnal temperature range (DTR) is not captured very well by the CTMD in spring and autumn (Gao et al., 2018a). We want to emphasize that the CTMD is only validated by 24 sites, which are mainly in low terrains. The credibility of the CTMD in the high peaks is difficult to evaluate because few observations exist. Nevertheless, we believe that the CTMD is still creditable since it could capture the distribution characteristics of temperatures as well as the general warming trends.

2.2 CMA05

According to the two basic characteristics for the diagnosis of mechanisms responsible for the EDW, regional warming amplification and altitude warming amplification is detected, respectively. The former feature is compared with other regions, such as plateaus, mountains, and low-altitude areas (basins and plains), to detect whether the warming trend in the mountain is greater. The latter focuses on the warming trend differences within the mountains (e.g., different altitude ranges), which is to determine whether warming amplification in the high-altitude areas is more significant than the low-altitude areas. To detect the regional warming amplification, the CMA05 was evaluated and compared with the CTMD.

The CMA05 dataset was produced by the China Meteorological Data Sharing Service System of the National Meteorological Information Centre (http://data.cma.cn/data/cdcdetail/dataCode/SURF_CLI_CHN_TEM_MON_GRID_0.5.html). It contains three monthly temperature indices (minimum, mean and maximum temperature) at the $0.5°$ latitude-longitude grid. The CMA05 is highly reliable and was widely applied for climatology studies since it was interpolated using Thin Plate Spline method based on high-density ground stations (approximately 2400 national meteorological observation stations) since 1961. The common time period 1979–2016 was extracted for the current study. Previous studies found that Qinghai-Tibetan Plateau (QTP) as the first step (highest) of China's terrain has a significant temperature warming trend over China (e.g. You et al., 2010). To reduce the warming influence, the QTP is eliminated. Thus, not only the whole continental China (hereafter referred to as WCC), but the low-altitude areas (hereafter referred to as LCC) that represented by excluding the CTM and the QTP from the WCC were also used for comparison.

2.3 Snow cover and snow depth data

To further discuss the possible hypotheses and mechanisms with respect to EDW, snow cover and snow depth data in the CTM are collected. The snow cover rate is calculated by dividing the snow cover area by the total area. The snow cover area was interpreted based on the MODIS/Terra Snow Cover 8-Day L3 product (MOD10A2, version 5) with a 500 m spatial resolution from the NASA Snow and Glacier Data Centre (https://nsidc.org/data/MOD10A2/versions/5). The annual maximum and minimum snow cover rates in the CTM from 2002 to 2013 were calculated, respectively. This data set was processed and provided by Chen et al (2016) and Deng et al (2019).

The daily snow depth data at 25 km spatial resolution from 1979-2016 over the CTM is derived from the National Earth System Science Data Center, National Science & Technology Infrastructure of China (Che 2015). The snow depth was calculated based on the original daily passive microwave brightness temperature data (EASE-Grid) produced from SMMR (1979-1987), SSM/I (1987-2007) and SSMI/S (2008-2019) of the National Snow and Ice Data Center (NSIDC). The detail information on the data production could be found in Che et al (2008), Dai et al (2015) and Dai et al (2017).

2.4 Analytical methods

In this study, the 6-hourly data of the CTMD was aggregated to the minimum temperature (Tmin), maximum temperature (Tmax), and mean temperature (Tmean) on monthly, seasonal, and annual time scales. A standard linear regression was applied to calculate the warming rate in each grid from 1979–2016 for the CTMD and CMA05 datasets, respectively. The corresponding equation is given by:

$$y = \alpha x + \beta \qquad\qquad (2)$$

where, y are the temperatures (Tmin, Tmax and Tmean) on different time scales, x is the time series from 1979-2016, and the fitting coefficient (slope) α indicates the warming rate. Thus, in this study, EDW is referring to the rate of warming over a multi-annual scale.

To detect the altitude warming amplification within the CTM, the whole altitude range is divided into 14 groups with a 500 m interval (Table 1). The number of grids in each group is also listed in Table 1. The standard linear regression was also used to assess different significance levels ($p<0.1$, $p<0.05$, $p<0.01$, $p<0.005$ and $p<0.001$) of EDW for different altitude groups. In such an analysis, y is the warming rate from 1979-2016 for each altitude group. Due to a different number of grids in each altitude group, the averaged warming rate of each group was used for the regression. x is the 14 altitude groups (natural positive integer 1 to 14). Thus, the fitting coefficient (slope) represents the magnitude of significance of EDW. The coefficient of determination (R^2) and confidence test (p-values) illustrate the goodness of the fit.

3 Results

185 **3.1 Regional warming amplification of the CTM**

The temperature trends on monthly, seasonal, and annual time scales with respect to Tmin, Tmax and Tmean were calculated via equation (2) based on aggregated Tmin, Tmax and Tmean from 6-hourly data of the CTMD for each grid. Table 2 shows the ratio of sum of grids at different significance level ($p<0.1$, $p<0.05$ and $p<0.01$) to total grids (356133) with respect to monthly temperatures. All grids reach the significant levels for Tmax in March, followed by 99.35% of all grids for Tmean.

190 The number of grids that reached the significance levels was the least in December, especially for Tmean and Tmax. For Tmin, more than half of the grids in only 2 months (March and June) reached the significance levels. For Tmean, 5 months (March, April, June, July and August) have exceeded 50% grids at the significance levels. For Tmax, only February and March has more than half of all grids at the significance levels. Although the temperature trend at some grids in certain month did not reach a statistical significant level, it can still reflect climate warming to a certain extent. Thus, the subsequent

195 analysis still depends on the temperature trend of each grid.

The annual and seasonal temperature trends in the CTM are weaker than those over the whole continental China (WCC) with respect to the mean temperature (Tmean), maximum temperature (Tmax), and minimum temperature (Tmin), except during spring (Table 3). The warming rates in spring Tmax and Tmin both exceed 0.6 °C 10a^{-1}, which is much higher than that of WCC and the low-altitude areas (LCC) that represented by excluding the CTM and the QTP from the whole continental

200 China. The summer Tmin and Tmean trends of CTM are also higher than that of LCC. The annual Tmin shows the greatest warming trend with a rate of 0.347 °C 10a^{-1}, followed by a Tmax and Tmean warming rate of 0.323 and 0.245 °C 10a^{-1}, respectively, in the CTM (Table 3). While summer has a much higher trend than autumn for Tmean and Tmin, it shows a comparable rate for Tmax (Table 3). Winter has the lowest rates compared with other seasons for the three temperature trends, with even a decreasing trend (-0.085 °C 10a^{-1}) observed for Tmean. In general, Tmin and Tmax show comparable

205 rates in spring. A more significant increment in Tmin compared with Tmax is observed in summer and autumn. However, the trends of CTM are consistent with the WCC and LCC, except winter Tmean (Table 3).

The warming rate varies from month to month, which is more significant than that from season to season. All temperature trends are negative in January and December in the CTM, which is different from that in WCC and LCC (Table 4). The decreasing rate is more significant in January than in December. It is worth noting that Tmax decreases slightly in May,

210 while Tmin warms significantly at a rate of 0.624 °C 10a^{-1} in the CTM. The largest warming rates are observed for both the CTM and land surface of China in March for all the temperature types. However, the CTM has a higher magnitude of warming rate. The warming trend is 1.339 °C 10a^{-1}, which is almost double than that over the whole of China (Table 4). Both rates exceed 0.8 °C 10a^{-1} for Tmean and Tmin in the CTM in March. April shows the second largest Tmax and Tmean warming trends in the CTM, which are also higher than that over continental China. For Tmin, May and June have rates

215 greater than 0.6 °C 10a^{-1}. The significant warming trends from March to May result in the higher trends in CTM than the

whole continental China, especially March (Table 4). In general, a more significant increment in Tmin is seen from March to June compared with the other months. March and April show remarkable warming trends for Tmax and Tmean (Table 4). In the entire CTM, Tmin warms faster than Tmax and Tmean. In general, regional warming amplification is significant in March and June for all temperatures. The trend for Tmax also increases faster in the CTM in February and April compared with the entire land surface of China. The warming rates in Tmean and Tmin in the CTM are faster than the WCC and LCC in April and May, respectively. All temperature trends on different time scales in the WCC are higher than LCC, which implies the warming rate of the Qinghai-Tibet Plateau contributes significantly to the national warming.

3.2 Warming amplification with altitude within the CTM

Because the performances of different temperature type (Tmin, Tmean and Tmax) are diverse for different months. We would select the months with the most significant temperature warming trends to illustrate the complexity and variability of EDW. To detect the altitude warming amplification features in the mountain areas, the CTM is divided into 14 groups with a 500 m altitude interval (Table 1). It is worth noting that the temperature trends in different elevation groups are significantly different compared with that of the entire CTM. Fig. 2 shows the Tmin trends at different elevations from 1979–2016 for four representative significant months (January, February, April, and December). As the number of grids in each elevation group is different, the boxplots show the inner-quantile range (25% to 75%) and median value. Meanwhile, linear regression is applied based on the average values, which indicate the altitude dependence of the warming trend (i.e. the significance of EDW). Since the monthly and seasonal temperature trends are calculated for each grid based on averaged 6-hourly data. Thus, to keep the consistent trend calculation for the whole study, the average value was used for the linear regression. In general, the EDW characteristics are significant for Tmin in January, February, April, and December. All lines of best fit are at the 0.001 significance level ($p<0.001$). The temperature trends are positive at altitudes higher than 5000 m, with the median values greater than 0 °C 10a^{-1} above 4000 m in January (Fig. 2a). The median values of most elevation groups are above the reference line in February, although the corresponding line of fit has a lower slope (0.033) compared with that of January (Fig. 2b). The 75% quantile ranges of the trends for all elevation groups in April are higher than 0 °C 10a^{-1} (Fig. 2c). All trends are positive for the regions nearly above 4000 m in April. The prevalence of EDW is most significant in December with the highest slope (0.064, $p<0.001$). Although, most lower altitude grids (<4000 m) show negative trends, the trends become positive at altitudes higher than 5000 m (Fig. 2d).

Although the slope (0.017) of the trend is not remarkable, a significant EDW trend ($p<0.001$) is seen for Tmax in March (Fig. 3a). Differing from that of April, August, and September, the same trend is observed for all elevation groups in March. Furthermore, all warming rates are greater than 0.8 °C 10a^{-1}. Significant elevation-dependent cooling can be found at the altitude range of 0–2500 m for Tmax in April. However, the temperature warming rate increases sharply (slope=0.069, $p<0.001$) with increment in the altitude from 2500 m to 7100 m. The median values are higher than 0.4 °C 10a^{-1} (Fig. 3b). Similar to April, EDW begins at a height of 4000–4500 m in August and September. However, the warming rates are greater

in September with the most positive values compared with August (Figs. 3c and 3d). In general, while Tmax warming is not widespread, it is more significant at higher elevations.

250   For Tmean, the EDW trend is most significant in January with the best significant level (slope=0.036, $p<0.001$, Fig. 3a). However, the warming rates in January are only slightly above 0 ℃ 10a^{-1} at higher elevations. Although February and March also show significant EDW at the 0.005 and 0.05 significant levels, respectively, the warming rates are much higher in March than in February with an average median value of approximately 0.8 ℃ 10a^{-1} (Figs. 4b and 4c). Significant EDW occurs above an elevation of 4500 m in August (slope=0.037, Fig. 4d). Table 5 summarizes monthly temperature trends over

255   different elevations based on CTMD from 1979-2016, especially the significant trend at higher elevations as showed in Figs. 2 to 4. The performances for all months and seasons are also provided in the supplementary material (Fig. S1-S13).

3.3 Spatial distribution pattern of the warming trend over the CTM

To better detect the altitude warming amplification feature, four typical zones with high mountains (above 3000 m) were selected, namely Zone 1 (represented by the Tolm Mountains), Zone 2 (central Tianshan, including the eastern part of the

260   Borokoonu Mountains), Zone 3 (represented by the Bogda Mountains), and Zone 4 (represented by the Balikun Mountains) (Fig. 5). The monthly minimum temperature trends of January in the higher altitude mountains are greater than the surrounding low-altitude areas, especially in Zones 3 and 4 (Fig. 5a). The highest warming trend (exceeding 1.0 ℃ 10a^{-1}) is found around the eastern Bogda Mountains (above 3000 m) in Zone 3. The lowland to the north of the Bogda Mountains shows a cooling trend (Fig. 5a). Zone 4 also shows a remarkable EDW phenomenon (0.3–0.6 ℃ 10a^{-1}), wherein high

265   mountains such as the Balikun are slight warmer than the surrounding lowlands. Although the warming trend of Zone 1 is not as distinct as that of Zones 3 and 4, compared with the Ili Valley (cooling trend), the warming rate is still remarkable (~0.4 ℃ 10a^{-1}). In December, the warming trend is more significant in Zone 1 compared with the other Zones (Fig. 5b). The trend in the Tolm Mountains (exceeding 0.4 ℃ 10a^{-1}) is much higher than that in the Ili Valley (cooling trend), which is located in the northern part of Zone 1. The warming rate at high altitudes in Zone 3 is higher (0.2–0.4 ℃ 10a^{-1}) than that in

270   the lowlands. There is no obvious warming amplification in the high-altitude mountains of Zone 4 compared with the low-altitude areas (Fig. 5b). However, it is worth noting that even in the same mountainous area, such as in the Bogda Mountains in Zone 3, the warming rate in the east is notable faster than that in the northwest. Beside, in order to more intuitively reveal the warming rate of temperature is amplified with elevation, a southwest-southeast direction terrain profile is created for Zone 2 for example. It is clear to found that the minimum temperature warming trends accelerate as elevation rising in

275   January and December. The warming trends become positive at around 3000 m altitude (Fig. 5).

The maximum temperature in March in the entire CTM warms significantly with rates ranging from 0.9 to 2.0 ℃ 10a^{-1} (Fig. 6a). The highest warming rate can be observed in the western Ili Valley. However, all typical zones show strong altitude warming amplification features. The areas above 4500 m in Zone 1 have trends higher than 1.4 ℃ 10a^{-1}. The smoothed

contour of 3000 m corresponds to a distinct boundary in Zone 2. The temperature warming rates are almost higher than ~1.5 °C 10a^{-1} in the areas above 3000 m, while the rates are smaller in the low altitude areas (Fig. 6a). The sub-plots illustrate the consistent trends between elevation and maximum temperature in Zone 2 (Fig. 6a). The trend is higher than ~1.1 °C 10a^{-1} in March, while the trend becomes positive at around 2000 m in September (Fig. 6b). The difference between the warming rates in the high-altitude and low-altitude areas is the most remarkable in Zone 3. The temperature warming trend on the hilltop of the Bogda Mountains is much higher than that at the foot of the mountains (Fig. 6a). The temperature warming rate in Zone 4 ranges from 1.3 to 1.6 °C 10a^{-1}. The trend differences between the high-altitude and low-altitude areas in Zone 4 are not as remarkable as those in Zone 3 (Fig. 6a). However, the warming rate on the hilltop is much higher than that in the neighbouring lowlands (Fig. 6a).

The spatial distribution of the maximum temperature in September shows a distinctive east-west differentiation. The warming rates in Zones 3 and 4 are greater than those in Zones 1 and 2 (Fig. 6b). The EDW feature is not notable in Zone 4. In contrast, the temperature in the high-altitude areas shows a slower warming trend (approximately 0.2–0.3 °C 10a^{-1}) than that in the low-altitude areas in Zone 3 (Fig. 6b). A slight EDW phenomenon can be seen in the Tolm Mountains in Zone 1. However, Zone 2 shows remarkable EDW in September compared with the other zones. Similar to March, areas above 3000 m warm faster than the lowlands, especially the Ili Valley (Fig. 6b). In summary, Zone 2 is found to be a significant EDW area in the maximum temperature for March and September.

Zones 1 and 4 tend to show the altitude warming amplification phenomenon for the monthly mean temperature in January (Fig. 7a). The temperature decreases (by approximately −0.2 to −0.4 °C 10a^{-1}) in the Ili Valley but increases (approximately 0.05 to 0.15 °C 10a^{-1}) in the Tolm Mountains, especially in the high-altitude areas (Fig. 7a). Zone 4 warms faster than the regions outside the zone. However, the warming trend is not notable in the high elevation areas compared with the lowlands within this zone (Fig. 7a). The temperatures show cooling trends in Zones 2 and 3. Nevertheless, the trend is amplified with elevation in January in Zone 2. The high-altitude areas are warmer than the low-altitude regions, especially in the Bogda Mountains of Zone 3 (Fig. 7a). The spatial distribution of the warming rate in February is similar to that in January. However, the trend in most areas of the CTM is positive (Fig. 7b). Zones 3 and 4 show obvious EDW phenomena in February. The difference between the temperature warming rates in the high and low terrains of these two zones exceeds 0.2 °C 10a^{-1}. The trend in the high terrains of Zone 2 is greater than that in the valleys in the western part of the zone (eastern Ili Valley). However, the temperature in the south of the zone is warming faster than in the high mountains in the northern part of Zone 2 (Fig. 7b). The temperature warming rate maintains a continuous growth in the altitude gradient along the terrain profile in Zone 2 in February (Fig. 7b). The southwestern Tolm Mountains in Zone 1 are warming up faster than the north-eastern mountains. In general, the warming trend of mean temperature is not as dramatic as that of the minimum and maximum temperatures in the CTM. The spatial distribution of warming trends for all months and seasons could be found in the supplementary material (Fig. S14-S30).

4 Discussion

Based on our analysis, it can be seen that the EDW phenomenon is very complicated for a large mountain system. It is hard to arbitrarily judge the prevalence of EDW in a mountain system. Based on comprehensive quantitative analysis, we believe that significant EDW signals exist in the CTM on local scales with respect to different temperature types. While previous studies have mainly focused on the EDW of annual and seasonal temperatures, the monthly scale has not received sufficient attention. However, seasonal temperatures do not clearly reflect the EDW characteristics. In complex terrains, monthly temperature changes are more significant, especially during season transitions. For example, rapid warming in March would accelerate the melting of ice and snow, affecting the glaciers and regional water resources in the mountains.

The air temperature changes are mainly affected by two aspects: one is the vertical energy exchange between the ground and atmosphere that leads to periodic changes on the daily and annual scales; the other is the temperature advection caused by the movement of the cooling and heating masses, which leads to non-periodic changes. Numerous studies shown that the atmospheric circulation not only affects the latitude and zonality of climate via the zonal distribution of circulation, but also expands the influence range of sea-land and topography via the energy and water transportation (Dickinson, 1983; Harding et al., 2001). It is worth noting that the temperature trend is always positive at an altitude of 4500 m or higher in the CTM. However, the temperature has a cooling trend in winter below 3000 m, especially Tmin (Fig. 2). The significant altitude warming amplification phenomenon only could be found above 4500 m for August Tmean (Fig. 3 and Table 5). The air at high altitudes is similar to the free atmosphere and the dry adiabatic process is dominant. The absorption and reflection of solar radiation by the surface mainly determine the temperature change. In low-altitude areas, the impact of underlying surface characteristics (e.g. terrain and land cover) is more significant. The CTM has a complex terrain with many mountain basins and canyons. Since the "Cold Lake" effect in winter, the lapse rate even is positive. A temperature inversion layer often happens in deep canyons at night. Meanwhile, in low-altitude areas, the more surface soil moisture results in latent heat fluxes increasing, which further causes more absorbed solar radiation and then temperature warming in winter (Rangwala et al., 2012). This mechanism is closely related to snowlines and treelines because the migration of snowline and treeline changes the surface albedo (Mountain Research Initiative EDW Working Group, 2015).

On a local scale, the ice and snow albedo, cloud cover, water vapor and radiation flux, and aerosols (including black carbon) are considered to be the main influence factors of EDW (Mountain Research Initiative EDW Working Group, 2015; Rangwala and Miller, 2012). However, whether clouds, water vapour and aerosols, the core mechanism is that they affect the absorption of solar short-wave radiation by the land surface and the long-wave radiation outward from the land surface (Shi et al., 2020; Zhang et al., 2018). The balance of surface energy is changed, which leads to increasing/decreasing near-surface air temperature. In other words, the surface energy balance is the key mechanism that affects seasonal and inter-annual changes of EDW (Rangwala and Miller, 2012).

Surface albedo is a comprehensive indicator of many factors that affect the surface energy balance. It is also the core factor and key variable that controls the surface energy budget (Dickinson, 1983; Harding et al., 2001; Wang et al., 2005). Many factors such as terrain, vegetation cover, ice and snow, soil moisture, soil physical properties, and meteorological conditions could affect surface albedo (Zhang et al., 2018). For high mountain regions, vegetation cover and ice/snow cover are the two most important factors (Dickinson, 1983; Zhang et al., 2016; Zhang et al., 2018). For the whole CTM, small glaciers are more sensitive to the warming climate. The estimated glacier mass loss could be -2.3×10^3 kg m^{-2} below 3000 m, especially in Zone 2 (Deng et al., 2019). The snow cover and its duration also show a decreasing trend (Sorg et al., 2012; Deng et al., 2019). Guo and Li (2015) found the decreasing trend of the ratio of snow fall to precipitation (S/P) in the CTM, especially in the four typical zones 1 to 4 in this study.

Deng et al (2019) found that the snow cover rate in the CTM decreased at a rate of 0.44% from 2002-2013. According to the snow cover rate data from Chen et al (2016) and Deng et al (2019), the maximum snow cover rate always occurred in January, while the minimum snow cover happened in July. We tested the relationship between monthly Tmin, Tmean and Tmax with maximum/minimum snow cover rate for each month in 2002-2013. Figure 8 shows the relationship of temperature and snow cover rate. Only February Tmin has a strong correlation (R^2=0.302, p<0.1) with the maximum snow cover rate (Fig. 8a). For minimum snow cover rate, Tmax in August has a significant correlation (R^2=0.256, p<0.1) with it (Fig. 8a). The correlation between temperature in other months and snow cover rate is not significant (not shown here).

The annual trend of snow depth over the CTM from 1979-2016 is -0.12 cm 10a^{-1}, which means the snow is accelerated melting. Except January (0.16 cm 10a^{-1}) and February (0.05 cm 10a^{-1}), snow depth decreases in other months ranged from -0.01 to 0.58 cm 10a^{-1}. The snow depth decreases the fastest in March with a rate of -0.58 cm 10a^{-1}, followed by April with a rate of -0.45 cm 10a^{-1}. Thus, spring has the highest decreasing trend of snow depth. However, the temperature warming trends are most significant in spring and March with respect to Tmin, Tmean and Tmax (Tables 3 and 4). The relationship between snow depth and temperature is further investigated in the CTM from 1979-2016 (Table 6). A significant correlation (p<0.01) could be found between Tmin and snow depth in March and June. For the couple of Tmean and snow depth, the remarkable correlation (p<0.01) also is found in March, June and August, respectively. The significant correlation (p<0.01) only could be found in December between Tmax and snow depth (Table 6). In cold months, for example, November and January, a relative significant correlation (p<0.05) can be found between Tmean/Tmax and snow depth. Figure 9 shows the scatter plots of comparison of Tmin and Tmean in March with snow depth. The negative correlation is perspicuous and visible. In general, there is a negative correlation between temperature and snow cover/snow depth (Figs. 8 and 9), which implies that the temperature warming has an promote effect on the accelerated melting of snow. Meanwhile, the accelerated melting of snow may affect the temperature warming. The detailed feedback mechanism between snow and temperature needs to be further verified and explored by using advanced technology and models. In summary, although many hypothetical mechanisms of EDW have received widespread attention, most of them are limited to phenomenon description

and qualitative analysis. The present study tried to do some preliminary explorations on the mechanism based on limited snow cover and snow depth data. There is a lack of quantitative investigation on the core processes, dominant factors as well as temporal-spatial differences of EDW.

5 Conclusions

Compared with the warming trend over the national land surface (WCC) and the low-altitude areas (LCC), the CTM is warming faster (0.633 and 0.640 °C $10a^{-1}$ for Tmin and Tmax, respectively) in spring (Table 3). However, on a monthly scale, the warming rates are more complicated. The warming trends of the three temperature indicators (Tmin, Tmax, and Tmean) in March (0.835 and 1.339 °C $10a^{-1}$ for Tmin and Tmax, respectively) and June (0.752 and 0.422 °C $10a^{-1}$ for Tmin and Tmax, respectively) in the CTM are higher than those over the entire national land surface on average (Table 4). Besides, the trends of Tmax in February, Tmax and Tmean in April, and Tmin in May are also higher than the national average. Therefore, EDW detection based on the monthly scale is more reasonable and accurate.

It cannot be simply concluded that the high-altitude areas are warming faster than the low-altitude areas. Quantitative analysis is necessary to provide solid evidence of the EDW phenomenon. Via altitude grouping and a linear regression model, we quantitatively determined the significance of EDW along with the detailed performance of the warming trends with respect to Tmin, Tmean and Tmax at different altitudes. In the case of Tmin, January, February, April, and December show significant EDW trends ($p<0.001$). The most significant EDW phenomenon is found in December (Table 5). In other words, Tmin is associated with strong EDW in winter. The warming rates of Tmin above 5000 m are always positive, which could lead to the faster melting of snow. March, April, August, and September show different elevation-based sensitivities with respect to Tmax. However, the significant EDW phenomenon can only be found at altitudes above 2500 m, 4000 m, and 4500 m in April, August, and September, respectively. The Tmax warming trends in March and April are always positive in the CTM. The cold months from January to March show significant EDW phenomena over the entire CTM with respect to Tmean. In August, the EDW phenomenon can be detected in areas higher than 4500 m.

The CTM is a large mountain system consisting of many mountains. Therefore, EDW characteristics are diverse in different mountains. The EDW of Tmin in January is significant in the Bogda and Balikun Mountains, while it is significant in December in the Tolm Mountains (Fig. 5). For Tmax in March, all the typical mountains exhibit EDW characteristics, especially the central CTM and Bogda Mountains (Fig. 6). A significant EDW signal of Tmax is observed in September in the central CTM (eastern part of the Borokoonu Mountains). The most significant EDW signal of Tmean is observed in the Tolm and Balikun Mountains in January. The Bogda and Balikun Mountains exhibit significant EDW features in February.

After preliminary research, the significant negative correlation ($p<0.001$) between minimum/mean temperature and snow depth are found in March and June (Fig. 9). However, the specific feedback mechanism between snow and temperature is

still unclear. Even in the same mountainous area, significantly different mechanisms of EDW are observed for different topographies, altitudes, and seasons. Future studies should focus on conducting in-depth quantitative research on the mechanism of EDW based on regional climate models and field surveys, especially in Zones 1 and 2 with accelerating snow melting.

6 Data availability

The data set is released at https://doi.org/10.1594/PANGAEA.887700 with a Network Common Data Form (NetCDF) format. The coverage of data set is 41.1814-45.9945 °N, 77.3484-96.9989 °E. The spatial resolution is 1km and the total number of grid point is 818126 for a larger Chinese Tianshan Mountains region (which includes more surrounding areas. This study used 356133 grids). The time step is 6-hourly at 00, 06, 12, and 18 UTC. The data set contains 288 NetCDF files and one user guidance file. The monthly temperature data set at 0.5 ° latitude-longitude grid (CMA05) over the continental China is provided by the China Meteorological Data Sharing Service System of the National Meteorological Information Center (http://data.cma.cn/data/cdcdetail/dataCode/SURF_CLI_CHN_TEM_MON_GRID_0.5.html, last access: 05 January 2021). The MODIS/Terra Snow Cover 8-Day L3 product (MOD10A2, version 5) for snow cover rate calculation is provided by the NASA Snow and Glacier Data Centre (https://nsidc.org/data/MOD10A2/versions/5, last access: 07 January 2021). The daily snow depth data is provided by National Earth System Science Data Center, National Science & Technology Infrastructure of China (http://www.geodata.cn, 05 January 2021).

Author contributions

L.G. designed the research and collected the data, H.D., X.L. and J.W. contributed to the data processing and analysis, L.G. wrote the manuscript, and M.M., X.C., Y.N.C., Z.L., J.G., Y.C. and M.L. contributed to the discussion.

Competing interests

The authors declare that they have no conflict of interest.

Additional information

More analysis figures could be found in the Supplementary material.

Acknowledgements

This study was supported by the National Natural Science Foundation of China (41501106, 41877167 and 41807159), the National Key Research and Development Program (2018YFE0206400 and 2018YFC1505805), the Research and Development Support Program of the China Institute of Water Resources and Hydropower Research (IWHR) (JZ0145B582017), the Scientific Projects from Fujian Provincial Department of Science and Technology (2019R1002-3), and the Outstanding Young Scientific Research Talents Cultivation Program, Education Department of Fujian Province. Dr. Jianhui Wei was supported financially by the German Research Foundation through funding of the AccHydro project (DFG-Grant KU 2090/11-1).

References

Beniston, M., and Rebetez, M.: Regional behavior of minimum temperatures in Switzerland for the period 1979-1993, Theoretical and Applied Climatology, 53, 231-243, 1996.

Che, T.: Long-term series of daily snow depth dataset in China (1979-2019), National Tibetan Plateau Data Center, 2015. DOI: 10.11888/Geogra.tpdc.270194. CSTR: 18046.11.Geogra.tpdc.270194.

Che, T., Li, X., Jin, R., Armstrong, R., and Zhang, T.J.: Snow depth derived from passive microwave remote-sensing data in China, Annals of Glaciology, 49, 145-154, 2008.

Chen, Y., Li, W., Deng, H., Fang, G., and Li, Z.: Changes in Central Asia's water tower: past, present and future, Scientific Reports, 6, 35458, 10.1038/srep35458, 2016.

Dai, L.Y., Che, T., and Ding, Y.J.: Inter-calibrating SMMR, SSM/I and SSMI/S data to improve the consistency of snow-depth products in China, Remote Sensing, 7(6), 7212-7230, 2015.

Dai, L.Y., Che, T., Ding, Y.J., and Hao, X.H.: Evaluation of snow cover and snow depth on the Qinghai–Tibetan Plateau derived from passive microwave remote sensing, The Cryosphere, 11(4), 1933-1948, 2017.

Deng, H., Chen, Y., and Li, Y.: Glacier and snow variations and their impacts on regional water resources in mountains, Journal of Geographical Sciences, 29(1): 84-100, 2019.

Diaz, H. F., and Bradley, R. S.: Temperature variations during the last century at high elevation sites, Climatic Change, 36, 253-279, 1997.

Diaz, H. F., and Eischeid, J. K.: Disappearing "alpine tundra" Köppen climatic type in the western United States, Geophysical Research Letters, 34, 2007.

Ding, Y., Liu, S., Li, J., and Shangguan, D.: The retreat of glaciers in response to recent climate warming in western China, Annals of Glaciology, 43, 97-105, 2006.

Dickinson, R. E.: Land surface processes and climate-surface albedos and energy balance, Advances in Geophysics, 25: 305-353, 1983.

Dong, D., Huang, G., Qu, X., Tao, W., and Fan, G.: Temperature trend–altitude relationship in China during 1963–2012, Theoretical and Applied Climatology, 122, 285-294, 2015.

Du, J.: Change of temperature in Tibetan Plateau from 1961 to 2000, Acta Geographica Sinica, 56, 682-690, 2001. (in Chinese)

Gao, L., Bernhardt, M., and Schulz, L.: Elevation correction of ERA-interim temperature data in complex terrain, Hydrology and Earth System Sciences, 16(12): 4661-4673, 2012.

Gao, L., Hao, L., and Chen, X.W.: Evaluation of ERA-interim monthly temperature data over the Tiberan Plateau, Journal of Mountain Science, 11(5): 1154-1168, 2014

Gao, L., Bernbardt, M., Schulz, K., and Chen, X.W.: Elevation correction of ERA-Interim temperature data in the Tibetan Plateau, International Journal of Climatology, 37(9): 3540-3552, 2017.

Gao, L., Wei, J., Wang, L., Bernhardt, M., Schulz, K., and Chen, X.: A high-resolution air temperature data set for the Chinese Tian Shan in 1979–2016, Earth System Science Data, 10, 2097-2114, 2018a.

Gao, Y., Chen, F., Lettenmaier, D. P., Xu, J., Xiao, L., and Li, X.: Does elevation-dependent warming hold true above 5000 m elevation? Lessons from the Tibetan Plateau, npj Climate and Atmospheric Science, 1, 2018b.

Harding, R.J., Gryning, S.E., Halldin, S., and Lloyd, C.R.: Progress in understanding of land surface/atmosphere exchanges at high latitudes, 70, 5-18, 2001.

Mountain Research Initiative EDW Working Group: Elevation-dependent warming in mountain regions of the world, Nature Climate Change, 5, 424-430, 2015.

Guo, L., and Li, L.: Variation of the proportion of precipitation occurring as snow in the Tian Shan Mountains, China, international journal of climatology, 35, 1379-1393, 2015.

Guo, D., Sun, J., Yang, K., Pepin, N., and Xu, Y.: Revisiting recent elevation-dependent warming on the Tibetan Plateau using satellite-based data sets, Journal of Geophysical Research, 124, 8511-8521, 2019.

480 Jungo, P., and Beniston, M.: Changes in the anomalies of extreme temperature anomalies in the 20[th]century at Swiss climatological stations located at different latitudes and altitudes, Theoretical and Applied Climatology, 69, 1-12, 2001.

Liu, X., and Hou, P.: Relationship between the climatic warming over the Qinghai -Xizang Plateau and its surrounding areas in recent 30 years and the elevation, Advances in Climate Change Research, 017, 245-249, 1998. (in Chinese)

Liu, X., Cheng, Z., Yan, L., and Yin, Z.: Elevation dependency of recent and future minimum surface air temperature trends 485 in the Tibetan Plateau and its surroundings, Global and Planetary Change, 68, 164-174, 2009.

Mcguire, C. R., Nufio, C. R., Bowers, M. D., and Guralnick, R. P.: Elevation-dependent temperature trends in the Rocky Mountain Front Range: changes over a 56- and 20-year record, PLOS ONE, 7, e44370, 2012.

Pepin, N., Deng, H., Zhang, H., Zhang, F., Kang, S., and Yao, T.: An examination of temperature trends at high elevations across the Tibetan Plateau: the use of MODIS LST to understand patterns of elevation-dependent warming, Journal of 490 Geophysical Research, 124, 5738-5756, 2019.

Rangwala, I., Barsugli, J., Cozzetto, K., Neff, J. and Prairie, J.: Mid-21st century projections in temperature extremes in the southern Colorado Rocky Mountains from regional climate models, Climate Dynamics, 39, 1823-1840, 2012.

Rangwala, I., Miller, J. R., and Xu, M.: Warming in the Tibetan Plateau: possible influences of the changes in surface water vapor, Geophysical Research Letters, 36, L06703, 2009.

495 Rangwala, I., and Miller, J. R.: Climate change in mountains: a review of elevation-dependent warming and its possible causes, Climatic Change, 114, 527-547, 2012.

Seidel, D. J., and Free, M.: Comparison of lower-tropospheric temperature climatologies and trends at low and high elevation radiosonde sites, Climatic Change, 59, 53-74, 2003.

Simmons, A. J., Willett, K. M., Jones, P. D., Thorne, P. W., and Dee, D. P.: Low-frequency variations in surface 500 atmospheric humidity, temperature, and precipitation: Inferences from reanalyses and monthly gridded observational data sets, Journal of Geophysical Research: Atmospheres, 115, D01110, doi:10.1029/2009jd012442, 2010.

Shi, Y., Liu, C., and Kang, E.: The glacier inventory of China, Annals of Glaciology, 50, 1-11, 2009.

Shi, T. L., Pu, W., Zhou, Y., Cui, J. C., Zhang, D. Z., and Wang, X.: Albedo of Black Carbon-Contaminated Snow Across Northwestern China and the Validation With Model Simulation, Journal of Geophysical Research: Atmospheres, 125, 2020.

505 Sorg, A., Bolch, T., Stoffel, M., Solomina, O. N., and Beniston, M.: Climate change impacts on glaciers and runoff in Tien Shan (Central Asia), Nature Climate Change, 2(10), 725-731, 2012.

Thakuri, S., Dahal, S., Shrestha, D., Guyennon, N., Romano, E., Colombo, N., and Salerno, F.: Elevation-dependent warming of maximum air temperature in Nepal during 1976–2015, Atmospheric Research, 228, 261-269, 2019.

Wang, K. C., Wang, P. C., Liu, J. M., Sparrow, M., Haginoya, S., and Zhou, X. J.: Variation of surface albedo and soil
510 thermal parameters with soil moisture content at a semi-desert site on the western Tibetan Plateau, Boundary-Layer Meteorology, 116(1), 117-129, 2005.

Wang, P., Tang, G., Cao, L., Liu, Q., and Ren, Y.: Surface air temperature variability and its relationship with altitude and latitude over the Tibetan Plateau in 1981-2010, Advances in Climate Change Research, 8, 313-319, 2012. (in Chinese)

Wang, Q., Fan, X., and Wang, M.: Recent warming amplification over high elevation regions across the globe, Climate
515 Dynamics, 43, 87-101, 2014.

Wang, S.S., Grant, R.F., Verseghy, D.L., and Black, T.A.: Modelling carbon dynamics of boreal forest ecosystems using the Canadian Land Surface Scheme, Climatic Change, 55(4), 451-477, 2002.

Zhang, C., Lu, D., Chen, X., Zhang, Y., Maisupova, B., and Tao, Y.: The spatiotemporal patterns of vegetation coverage and biomass of the temperate deserts in Central Asia and their relationships with climate controls, Remote Sensing of
520 Environment, 175, 271-281, 2016.

Zhang, Y. L., Kang, S. C., Sprenger, M., Cong, Z. Y., Gao, T. G., Li, C. L., Tao, S., Li, X. F., Zhong, X. Y., Xu, M., Meng, W. J., Neupane, B., Qin, X., and Sillanpaa, M.: Black carbon and mineral dust in snow cover on the Tibetan Plateau, The Cryosphere, 12(2), 413-431, 2018.

Xu, M., Kang, S., Wu, H., and Yuan, X.: Detection of spatio-temporal variability of air temperature and precipitation based
525 on long-term meteorological station observations over Tianshan Mountains, Central Asia, Atmospheric Research, 203, 141-163, 2018.

Yan, L., andLiu, X.: Has climatic warming over the Tibetan Plateau paused or continued in recent years? Journal of Earth, Ocean and Atmospheric Sciences, 1, 13-28, 2014.

530 You, Q., Kang, S., Pepin, N., Flugel, W., Yan, Y., Behrawan, H., and Huang, J.: Relationship between temperature trend magnitude, elevation and mean temperature in the Tibetan Plateau from homogenized surface stations and reanalysis data, Global and Planetary Change, 71, 124-133, 2010.

Zhang, C., Lu, D., Chen, X., Zhang, Y., Maisupova, B., and Tao, Y.: The spatiotemporal patterns of vegetation coverage and biomass of the temperate deserts in Central Asia and their relationships with climate controls, Remote Sensing of Environment, 175, 271-281, 2016.

535 Zhang, Y. L., Kang, S. C., Sprenger, M., Cong, Z. Y., Gao, T. G., Li, C. L., Tao, S., Li, X. F., Zhong, X. Y., Xu, M., Meng, W. J., Neupane, B., Qin, X., and Sillanpaa, M.: Black carbon and mineral dust in snow cover on the Tibetan Plateau, The Cryosphere, 12(2), 413-431, 2018.

Table 1. Altitude groups over the CTMD.

	Altitude range (m)	Grid number
1	<500	3139
2	500–1000	30810
3	1000-1500	83018
4	1500-2000	70229
5	2000-2500	46545
6	2500-3000	43400
7	3000-3500	39579
8	3500-4000	28256
9	4000-4500	8789
10	4500-5000	1666
11	5000-5500	496
12	5500-6000	150
13	6000-6500	54
14	>6500	4

540

Table 2. Ratio of sum of grids at different significance levels ($p<0.1$, $p<0.05$ and $p<0.01$) to total grids (356133).

	Tmin	Tmean	Tmax
January	3.28	3.65	6.48
February	9.66	0.55	56.65
March	52.02	99.35	100.00
April	3.76	69.16	46.36
May	46.97	29.21	7.63
June	80.33	92.37	49.63
July	46.86	51.97	38.82
August	35.58	56.37	40.84
September	19.87	47.77	35.32
October	11.78	25.52	11.41
November	12.00	14.07	14.12
December	0.38	0.00	0.00

545 **Table 3. Annual and seasonal temperature trends (°C 10a^{-1}) in the CTM (based on CTMD) and the whole continental China (WCC) and low-altitude areas (LCC) by excluding the CTM and the QTP from the WCC (both based on CMA05) from 1979–2016.**

	CTM			WCC			LCC		
	Tmin	Tmean	Tmax	Tmin	Tmean	Tmax	Tmin	Tmean	Tmax
Spring	0.633 ***	0.522 ***	0.640 ***	0.557 ***	0.513 ***	0.518 ***	0.543 ***	0.498 ***	0.505 ***
Summer	0.441 ***	0.342 ***	0.266 **	0.472 ***	0.388 ***	0.378 ***	0.404 ***	0.336 ***	0.348 ***
Autumn	0.302	0.200 *	0.270	0.551 ***	0.458 ***	0.420 ***	0.506 ***	0.411 ***	0.371 ***
Winter	0.014	-0.085	0.115	0.432 ***	0.361 ***	0.327 ***	0.333 **	0.257	0.211
Annual	0.347 ***	0.245 ***	0.323 ***	0.503 ***	0.430 ***	0.411 ***	0.446 ***	0.376 ***	0.359 ***

Note: the bold and underlined value indicates a greater warming trend in the CTM than WCC and LCC. * denotes the significance level $p<0.1$, ** denotes the significance level $p<0.05$, and *** denotes the significance level $p<0.01$.

550

Table 4. Monthly temperature trends (°C 10a^{-1}) in the CTM (based on CTMD) and the whole continental China (WCC) and low-elevation areas (LCC) by excluding the CTM and the QTP from the WCC (both based on CMA05) from 1979–2016.

	CTM			WCC			LCC		
	Tmin	Tmean	Tmax	Tmin	Tmean	Tmax	Tmin	Tmean	Tmax
January	-0.133	-0.269	-0.235	0.343 [**]	0.256	0.212	0.225	0.143	0.102
February	0.313	0.177	**0.605** [**]	0.558 [***]	0.523 [***]	0.549 [**]	0.486 [**]	0.456 [*]	0.475 [*]
March	**0.835** [**]	**0.818** [***]	**1.339** [***]	0.651 [***]	0.672 [***]	0.752 [***]	0.661 [***]	0.673 [***]	0.738 [***]
April	0.441	**0.537** [***]	**0.664** [*]	0.547 [***]	0.522 [***]	0.516 [***]	0.520 [***]	0.503 [***]	0.508 [***]
May	**0.624** [**]	0.211	-0.082	0.475 [***]	0.345 [***]	0.284 [***]	0.447 [***]	0.317 [***]	0.270 [***]
June	**0.752** [***]	**0.476** [***]	**0.422** [***]	0.516 [***]	0.390 [***]	0.344 [***]	0.467 [***]	0.348 [***]	0.320 [***]
July	0.227	0.331 [***]	0.28	0.472 [***]	0.411 [***]	0.416 [***]	0.402 [***]	0.343 [***]	0.359 [***]
August	0.342	0.217 [*]	0.095	0.429 [***]	0.363 [***]	0.375 [***]	0.343 [***]	0.318 [***]	0.363 [***]
September	0.246	0.237	0.33	0.559 [***]	0.486 [***]	0.495 [***]	0.517 [***]	0.445 [***]	0.456 [***]
October	0.273	0.18	0.227	0.524 [***]	0.434 [***]	0.398 [***]	0.496 [***]	0.407 [***]	0.372 [**]
November	0.386	0.183	0.252	0.569 [***]	0.455 [***]	0.368 [**]	0.503 [***]	0.381 [**]	0.285
December	-0.137	-0.164	-0.025	0.394 [***]	0.303 [**]	0.219	0.287 [*]	0.171	0.055

Note: the bold and underlined value indicates a greater warming trend in the CTM than WCC and LCC. [*] denotes the significance level $p<0.1$, [**] denotes the significance level $p<0.05$, and [***] denotes the significance level $p<0.01$.

Table 5. Monthly temperature trends (°C 10a^{-1}) over different elevations based on the CTMD from 1979–2016.

	Tmin	Tmean	Tmax
January	0.039***	0.036***	0.037***
February	0.033***	0.012	0.008***
March	0.023	0.009**	0.017***
April	0.021***	-0.02***	**0.069*****
May	-0.056***	-0.022***	-0.045***
June	-0.025***	0.007	-0.046***
July	0.0	-0.017**	-0.019**
August	-0.011	**0.037*****	**0.023*****
September	-0.006	**0.017****	**0.038*****
October	-0.073***	-0.018***	**0.017****
November	-0.032***	-0.031***	-0.018***
December	0.064***	**0.006****	-0.018***

Note: the bold and underlined value indicates a warming trend at higher altitudes, rather than the whole altitude range. More details could be found in Figure 2 to 4 and Figure S1 to S12. * denotes the significance level $p<0.1$, ** denotes the significance level $p<0.05$, and *** denotes the significance level $p<0.01$.

Table 6. Relationship (R^2) of snow depth (cm) and monthly Tmin, Tmean and Tmax from 1979-2016.

	Tmin	Tmean	Tmax
January	0.021	0.098 *	0.109 **
February	0.031	0.050	0.103 *
March	0.399 ***	0.400 ***	0.033
April	0.003	0.076	0.008
May	0.086 *	0.104 *	0.012
June	0.194 ***	0.230 ***	0.095 *
July	0.081 *	0.108 *	0.016
August	0.047	0.242 ***	0.083 *
September	0.001	0.072	0.150 **
October	0.010	0.020	0.103 *
November	0.051	0.125 **	0.151 **
December	0.014	0.159 **	0.200 ***

Note: * denotes the significance level $p<0.1$, ** denotes the significance level $p<0.05$, and *** denotes the significance level $p<0.01$.
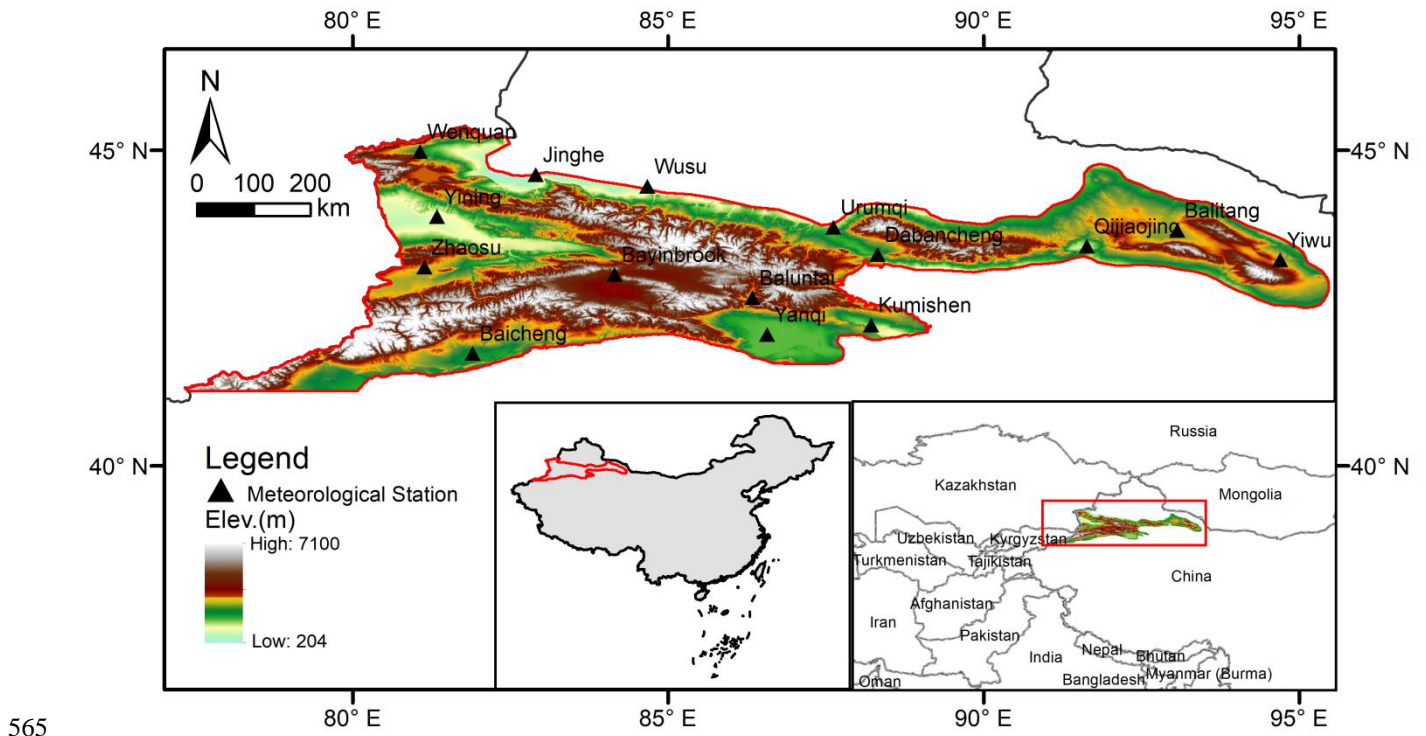
565

Figure1: Location of the Chinese Tianshan Mountains (CTM).The elevation ranges from 204 m to 7100 m a.s.l., with a DEM resolution of 1 km from SRTM. The grey sub-plot show the extent of the CMA05 at 0.5 °×0.5 °grid.
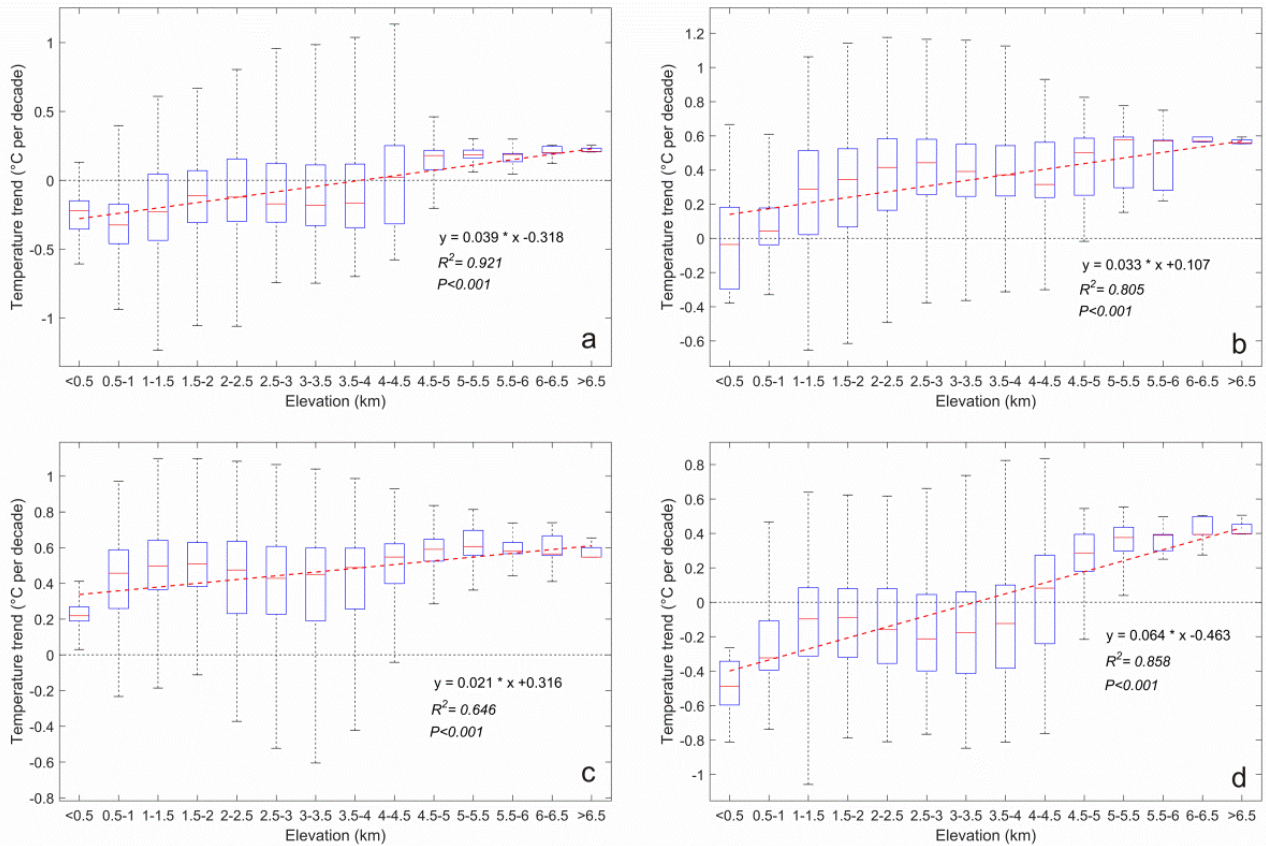
Figure 2: Box plots of monthly minimum temperature trends at different elevations from 1979–2016. (a) January, (b) February, (c) April, and (d) December. Thick horizontal lines in boxes show the median values. Boxes indicate the inner-quantile range (25% to 75%) and the whiskers show the full range of the values. The red dashed lines represent the significance of EDW.
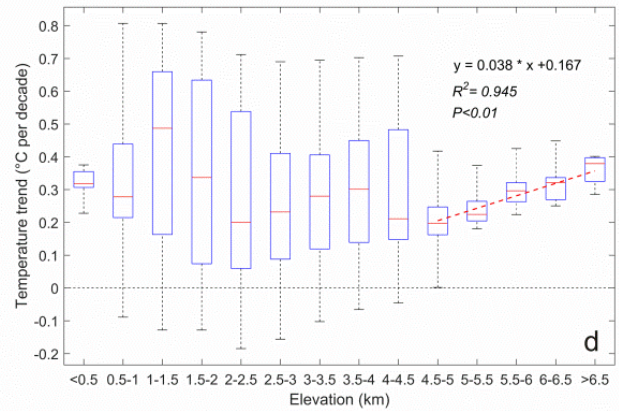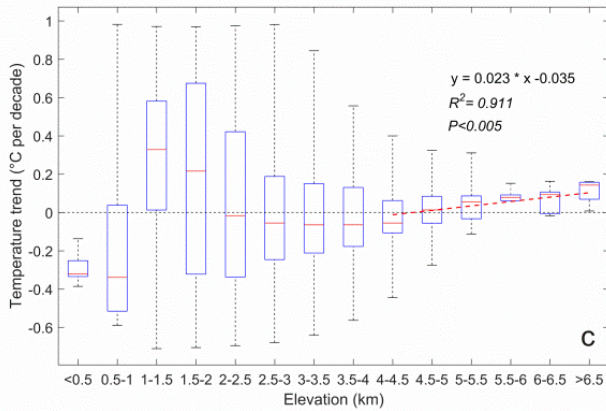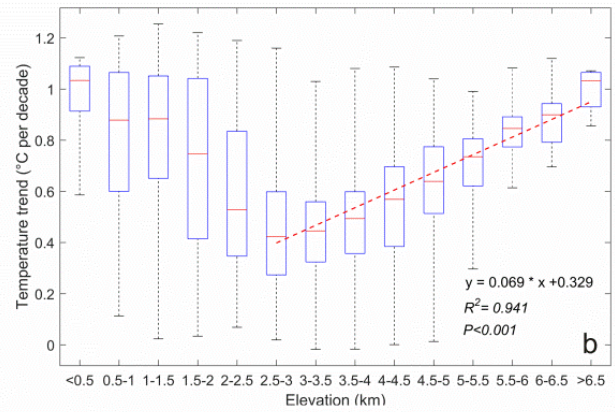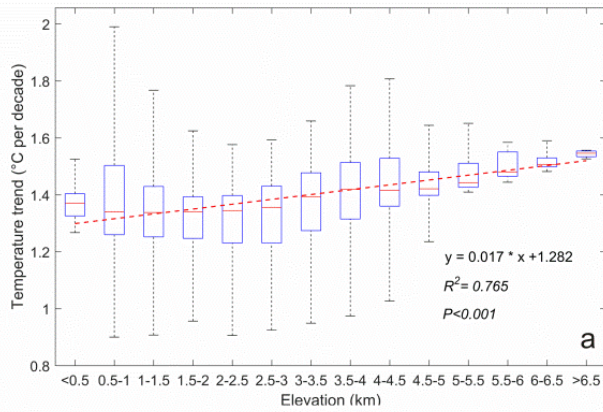
575

Figure 3: Box plots of monthly maximum temperature trends at different elevations from 1979–2016. (a) March, (b) April, (c) August, and (d) September. Thick horizontal lines in boxes show the median values. Boxes indicate the inner-quantile range (25% to 75%) and the whiskers show the full range of the values. The red dashed lines represent the significance of EDW.

580
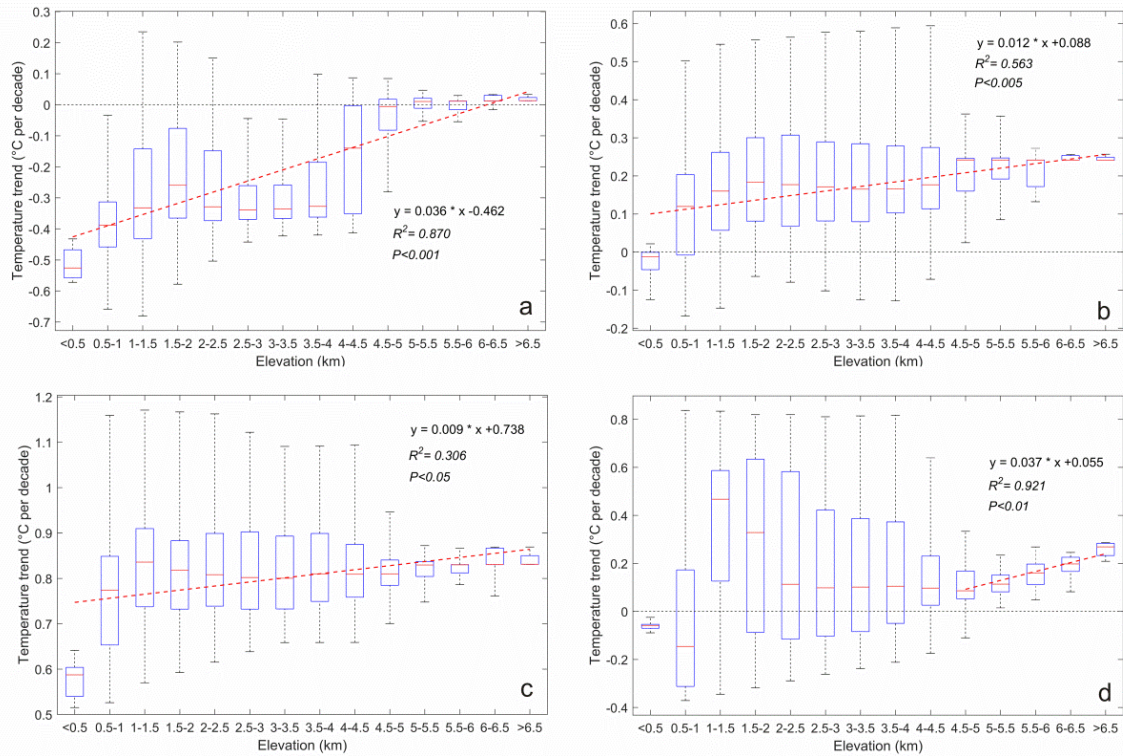
Figure 4: Box plots of monthly mean temperature trends at different elevations from 1979–2016. (a) January, (b) February, (c) March, and (d) August. Thick horizontal lines in boxes show the median values. Boxes indicate the inner-quantile range (25% to 75%) and the whiskers show the full range of the values. The red dashed lines represent the significance of EDW.
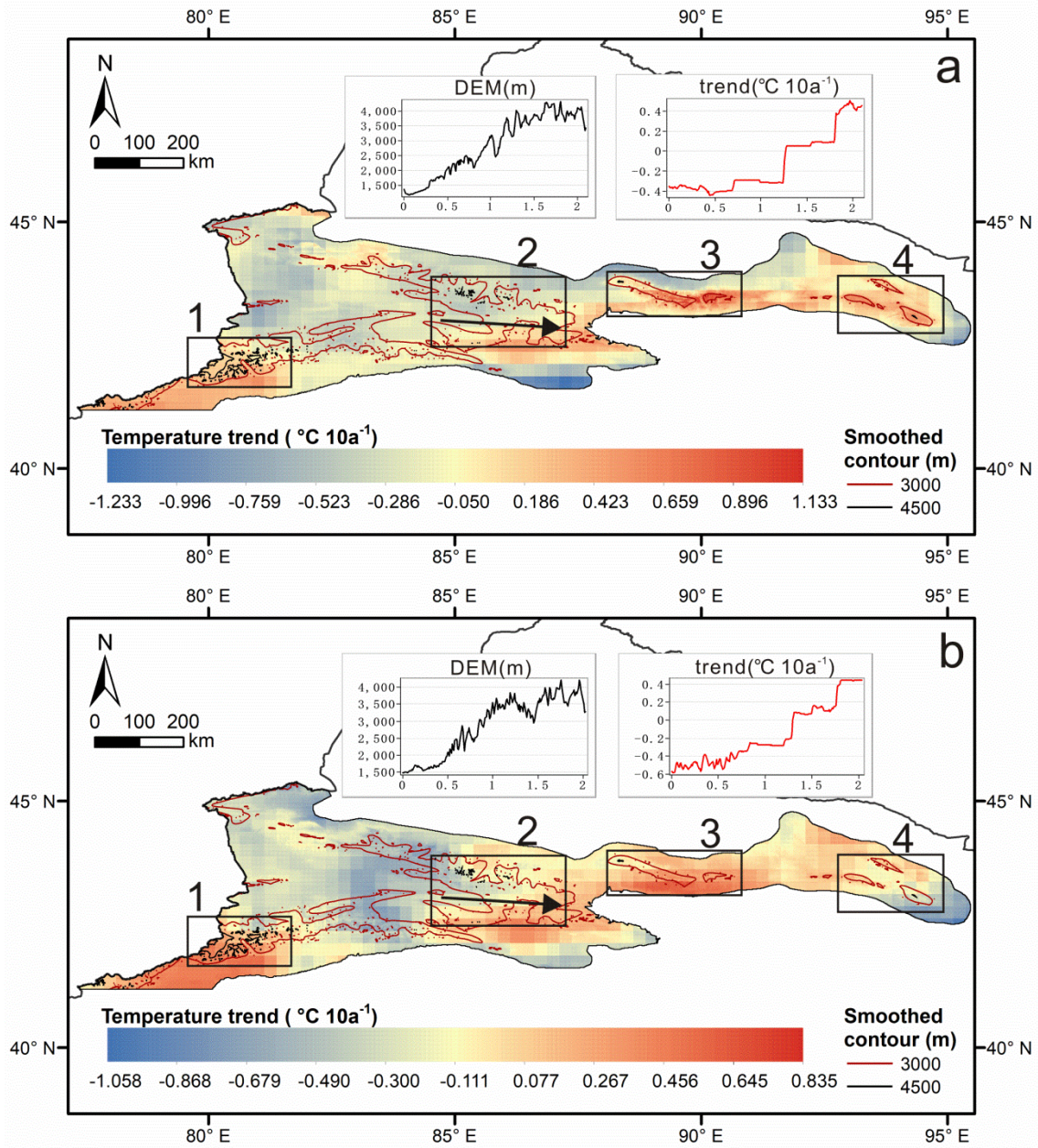
Figure 5: Monthly minimum temperature trends (a) January and (b) December for the entire CTM from 1979–2016. The ordinate of two sub-plots show the elevation trend and temperature trend along the terrain profile (black arrow indicates the direction) in Zone 2, respectively. The abscissa represents the distance in multiples of the scale.
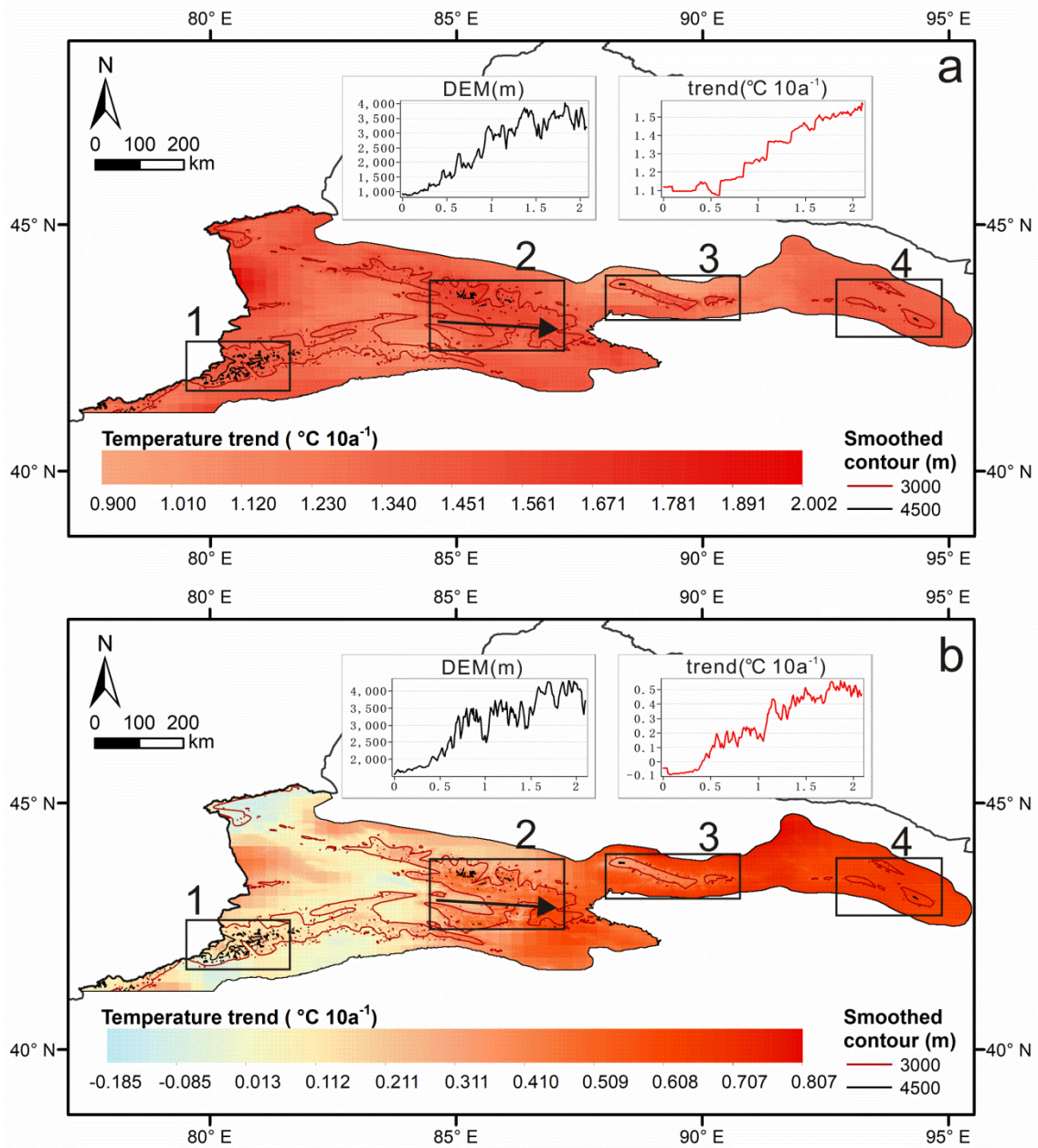
Figure 6: Monthly maximum temperature trends (a) March and (b) September for the entire CTM from 1979–2016. The ordinate of two sub-plots show the elevation trend and temperature trend along the terrain profile (black arrow indicates the direction) in Zone 2, respectively. The abscissa represents the distance in multiples of the scale.
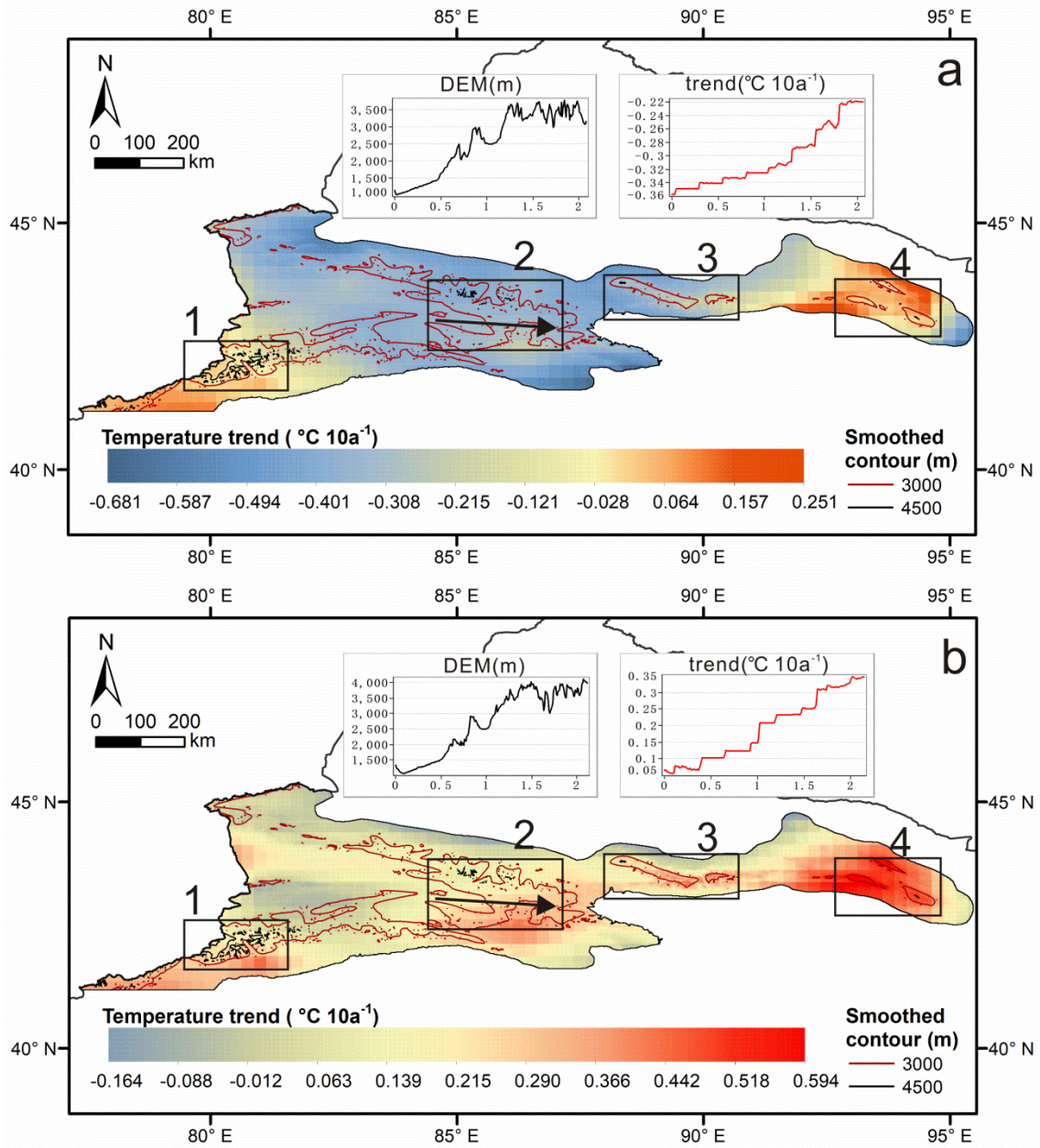
Figure 7: Monthly mean temperature trends (a) January and (b) February for the entire CTM from 1979–2016. The ordinate of two sub-plots show the elevation trend and temperature trend along the terrain profile (black arrow indicates the direction) in Zone 2, respectively. The abscissa represents the distance in multiples of the scale.
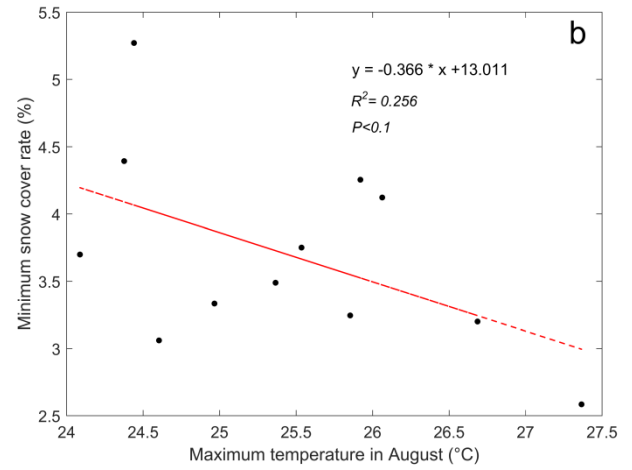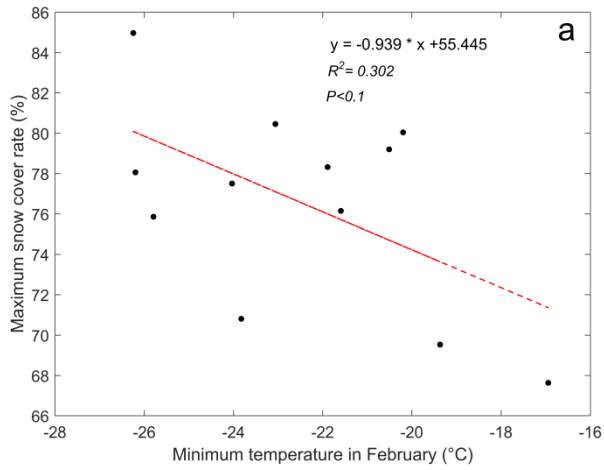
Figure 8: Relationship of temperature and snow cover rate (a) minimum temperature in February vs. maximum snow cover rate and (b) maximum temperature in August vs. minimum snow cover rate from 2002-2013.

605
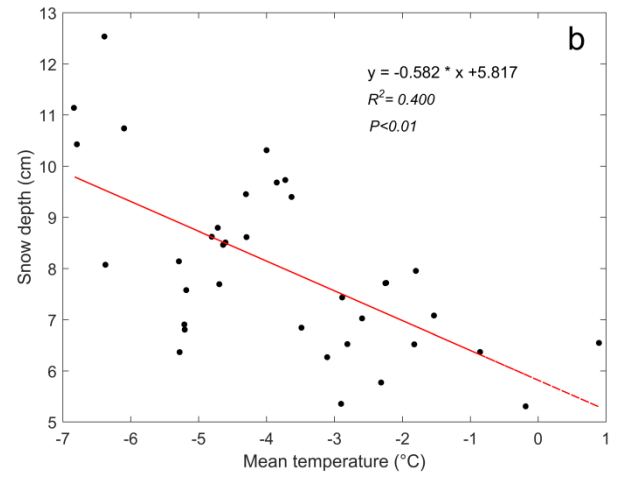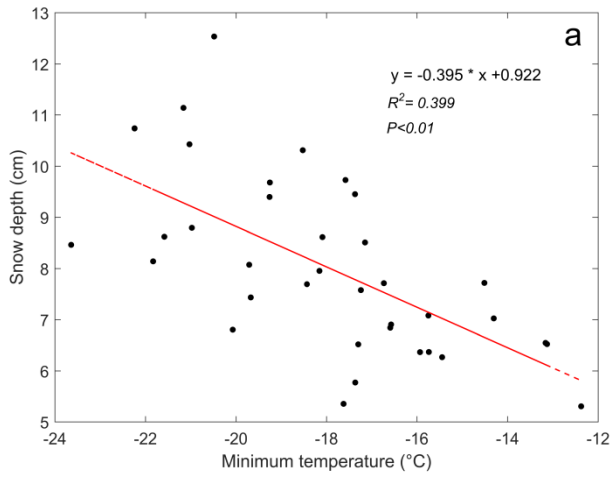
Figure 9: Relationship of snow depth and (a) Tmin in March and (b) Tmean in March from 1979-2016.